Journal of Materiomics 9 (2023) 892–898

Contents lists available at ScienceDirect

Journal of Materiomics

journal homepage: www.journals.elsevier.com/journal-of-materiomics/

Intrinsic ferroelectrics and carrier doping-induced metallic multiferroics in an atomic wire

Tao Xu [a, b, 1], Jingtong Zhang [c, d, 1], Chunyu Wang [e], Xiaoyuan Wang [e], Takahiro Shimada [b], Jie Wang [c, d, *], Hongxin Yang [a, **]

[a] Ningbo Institute of Materials Technology and Engineering, Chinese Academy of Sciences, Ningbo, 315201, China
[b] Department of Mechanical Engineering and Science, Kyoto University, Nishikyo-ku, Kyoto, 615-8540, Japan
[c] Department of Engineering Mechanics, School of Aeronautics and Astronautics Zhejiang University, Hangzhou, 310027, China
[d] Zhejiang Laboratory, Hangzhou, 311100, Zhejiang, China
[e] Key Laboratory of Pressure Systems and Safety Ministry of Education, East China University of Science and Technology, Shanghai, 200237, China

ARTICLE INFO

Article history:
Received 5 January 2023
Received in revised form
31 January 2023
Accepted 14 February 2023
Available online 21 March 2023

Keywords:
1D materials
Ferroelectrics
Metallic multiferroics
First-principles calculations
Electron doping

ABSTRACT

Low-dimensional multiferroic metals characterized by the simultaneous coexistence of ferroelectricity, conductivity, and magnetism hold tremendous potential for scientific and technological endeavors. However, the mutually exclusive mechanisms among these properties impede the discovery of multifunctional conducting multiferroics, especially at the atomic-scale. Here, based on first-principles calculations, we design and demonstrate intrinsic one-dimensional (1D) ferroelectrics and carrier doping-induced metallic multiferroics in an atomic WOF_4 wire. The WOF_4 atomic wire that can be derived from a 1D van der Waals crystal exhibits pronounced ferroelectricity manifested in the form of large cooperative atomic displacements. By performing Monte Carlo simulations with an effective Hamiltonian method, we obtain the nanowire that can sustain a high Curie temperature, indicating its potential for room-temperature applications. Moreover, doping with electrons is found to induce magnetism and metallic conductivity that coexists with the ferroelectric distortion in the nanowire. These appealing properties in conjunction with the experimental feasibility enable the doped WOF_4 nanowire to act as a promising atomic-scale multifunctional material.

1. Introduction

Ferroelectrics, characterized by a switchable spontaneous polarization, have been the subject of intensive research due to their broad technological applications, such as sensors, nonvolatile random-access memory (FeRAM), and so forth [1–3]. Driven by the surging demand for miniaturized electronic devices and the discovery of versatile exotic physical properties, tremendous research efforts have been devoted to the investigations of nanoscale ferroelectrics [4–8]. However, ferroelectricity is completely suppressed below the critical thickness of several nanometers in conventional ferroelectrics [9,10] due to the enhanced depolarizing field. The rise of 2D van der Waals (vdW) materials is a promising approach to circumvent this challenge and provides a platform for a new generation of the atomic-scale ferroelectrics. A series of intrinsic 2D ferroelectric materials have been explored recently embarked by the observation of stable electric polarization in monolayer SnTe [11], which include but not limited to MX_2 (M = W, Mo, X = S, Se, Te) transition metal dichalcogenides (TMDs) [12], group-IV monochalcogenides (GeS, GeSe, SnS, and SnSe) [13], buckled honeycomb compounds [14]. These atomic-scale ferroelectrics are endowed with superior ferroelectric, mechanical, electronic, and optical properties, and thus hold promise for the application of ultrahigh density electronic devices with low energy consumption and high performance.

In accordance with this promising route, it is highly desirable to extend the current low-dimensional ferroelectric studies to 1D ferroelectrics with robust polar order, which would enable a much higher density data storage compared with 2D ferroelectrics. 1D materials have demonstrated unique and various physics, such as Peierls transition [15], nontrivial band topology [16], and

* Corresponding author. Department of Engineering Mechanics, School of Aeronautics and Astronautics Zhejiang University, Hangzhou, 310027, China
** Corresponding author.
E-mail addresses: jw@zju.edu.cn (J. Wang), hongxin.yang@nimte.ac.cn (H. Yang).
Peer review under responsibility of The Chinese Ceramic Society.
[1] T.X. and J.T.Z. contributed equally to this work.

https://doi.org/10.1016/j.jmat.2023.02.012

superconductivity, as well [17]. Recently, hundreds of 1D weakly bonded van der Waals crystals have been identified through a novel data mining algorithm, which offers a comprehensive database to explore promising 1D atomic wire candidates with new functionalities. Besides, a few 1D ferroelectric atomic wires have been reported theoretically [18–20]. Despite the progress, the development of 1D ferroelectrics remains in the very early stage.

On the other hand, the recent interest in low-dimensional ferroelectrics not only lies in ferroelectricity itself but also extends to its coupling with other common degrees of freedom, such as strain, charge, spin, *etc*. These coupling effects open up unprecedented opportunities for the development of a plethora of multi-functional materials simultaneously holding ferroelectric, magnetic, and optical properties, which are quite promising for novel nanoscale electronics and new technological paradigms. However, single-phase materials possessing such coupling are very challenging to realize and are rarely explored in low-dimensional materials because of mutually exclusive mechanisms. Specifically, both free electrons and reduced dimensions are believed to destroy ferroelectricity, let alone the seemingly incompatibility between ferroelectricity and ferromagnetism. The discovery of 1D multiferroic metals will not only reveal new physical mechanism behind them but also facilitate the development of multifunctional nanodevices.

In this work, we predict that the WOF_4 nanowire with electrostatic doping is a one-dimensional multiferroic metal. Structural, ferroelectric, and electronic properties of one-dimensional WOF_4 atomic lines are studied in terms of the density functional theory and the modern Berry phase approach of ferroelectric calculation. The exfoliation energy, phonon spectra, molecular dynamics simulations, and Monte Carlo simulations indicate that the WOF_4 atomic wire is a stable 1D ferroelectric with large polarization, which is manifested in the form of large cooperative atomic displacements. Moreover, doping with electrons is found to induce magnetism and metallic conductivity that coexist with the ferroelectric distortion in the nanowire.

2. Simulation method

Our first-principles calculations are performed based on the density functional theory within the VASP code [21,22]. The exchange-correlation interaction is treated with the generalized gradient approximation (GGA) [23] of the Perdew-Burke-Ernzerhof (PBE) functional [24]. A $1 \times 1 \times 15$ Monkhorst-Pack *k*-point scheme is used for Brillouin zone integrations and a plane-wave cutoff of 520 eV is employed for the electronic wave function. The Grimme's DFT-D3 approach is imposed for the van der Waals correction. The axial lattice constant of the nanowire and the atomic positions are fully relaxed until the force on each atom is less than 0.01 eV/Å. The Heyd–Scuseria–Ernzerhof (HSE06) screened hybrid functional [25,26] is employed to calculate the ferroelectric and electronic properties of the electron-doped nanowire, which has been proved to correctly reproduce the structural parameters of wide-gape oxides [27–29], and is indispensable for the accurate description of the electronic structures of charge imbalanced systems [30,31]. We adopt the common supercell approach with periodic boundary conditions as implemented in the VASP to perform electronic structure calculations. To model the nanowire, a vacuum thickness more than 20 Å is set to avoid the interactions between neighboring supercells due to the periodic boundary conditions. The climbing image nudged elastic band (CI-NEB) method approach [32] is adopted to determine the minimum energy pathway of the phase transition. The phonon dispersion curves are calculated by the finite displacement method using the PHONOPY code [33]. *Ab initio* molecular dynamics (AIMD) simulations with the NVT ensemble are performed to evaluate the thermal stability of the nanowire. An effective Hamiltonian model is built to investigate the temperature dependence of the ferroelectric properties. This method has been widely used to predict temperature-dependent polarization of many ferroelectrics, which is computationally efficient with accuracy comparable with the *ab initio* MD simulation. The details of the model and the related expansion parameters are provided in the Supplementary Material.

3. Results and discussion

3.1. Structural stability

The bulk WOF_4 is derived from the Materials Project database [34] and crystalizes in a tetragonal lattice with the *I*4 space group, as displayed in Fig. 1(a). The structure consists of weakly bonded 1D molecular chains, which have also been screened as 1D van der Waals (vdW) bulks in recent high-throughput calculations [35,36] and investigated very recently [37]. The initial configuration of WOF_4 atomic wire is exfoliated from the bulk WOF_4 and then the lattice constant *c* and atomic positions are fully relaxed. The optimized nanowire structure is shown in Fig. 1(b), in which the primitive unit cell denoted by the dashed red line belongs to a space group of *P*4. Each W atom locates in the octahedral holes formed by the framework of two axial O atoms and four in-plane F atoms. The W atom shifts towards one of the bridging O atoms along the axial direction, leading to the formation of two non-equivalent W–O bonds. The optimized lattice constant *c* (*i.e*., axial parameter) is 3.97 Å. The nanowire shows little crystal structure variation compared to the bulk counterpart, attributed to the weak vdW interaction between neighboring NWs.

The exfoliation energy E_{exf}, based on the formula of $E_{exf} = E_n/N_n - E_{bulk}/N_{bulk}$, is calculated to evaluate the thermodynamic stability of ground-state structure, where E_n and E_{bulk} are energies of nanowire and bulk WOF_4, and N_n and N_{bulk} are the number of atoms in the nanowire and bulk materials, respectively. The obtained formation energy is around 68 meV per atom, which is not only lower than those of other theoretically proposed NW, including $NbOI_3$ [19], and experimentally obtained 1D nanowire like SnTe [38], but is also comparable to those of 2D materials (*e.g.* graphene (~52 meV per atom) and MoS_2 (77 meV per atom) [39]). This indicates that the exfoliation of WOF_4 nanowire from the bulk is highly possible. Furthermore, we verify the dynamic stability of the nanowire by calculating the phonon dispersion, and the result is shown in Fig. 1(c). It is evident that the nanowire is free from any imaginary phonon modes throughout the Brillouin zone. We also performed the *ab initio* MD simulations at 300 K for 5 ps. As shown in Fig. 1(d), the nanowire remains intact and shows tiny structure distortions, and the total energy of the simulation system keeps oscillating around an equilibrium position during the simulation, which suggests that the nanowire can be stable above room temperature. These results indicate that the WOF_4 nanowire is stable and experimentally accessible.

3.2. Spontaneous polarization

Having assessed the stability of the nanowire, we proceed to probe the ferroelectricity of the nanowire. The WOF_4 nanowire exhibits obvious structural symmetry breaking due to the large off-center displacements of the W atoms along the NW direction in an octahedron, which is reminiscent of the structure of ferroelectric perovskite oxides such as $BaTiO_3$ [40] and $PbTiO_3$ [41]. Evidently, the centers of the positive and negative charges do not coincide in the nanowire, leading to a spontaneous polarization along the nanowire direction. Note that the corresponding depolarization field is also along the axial direction in this case, which thus

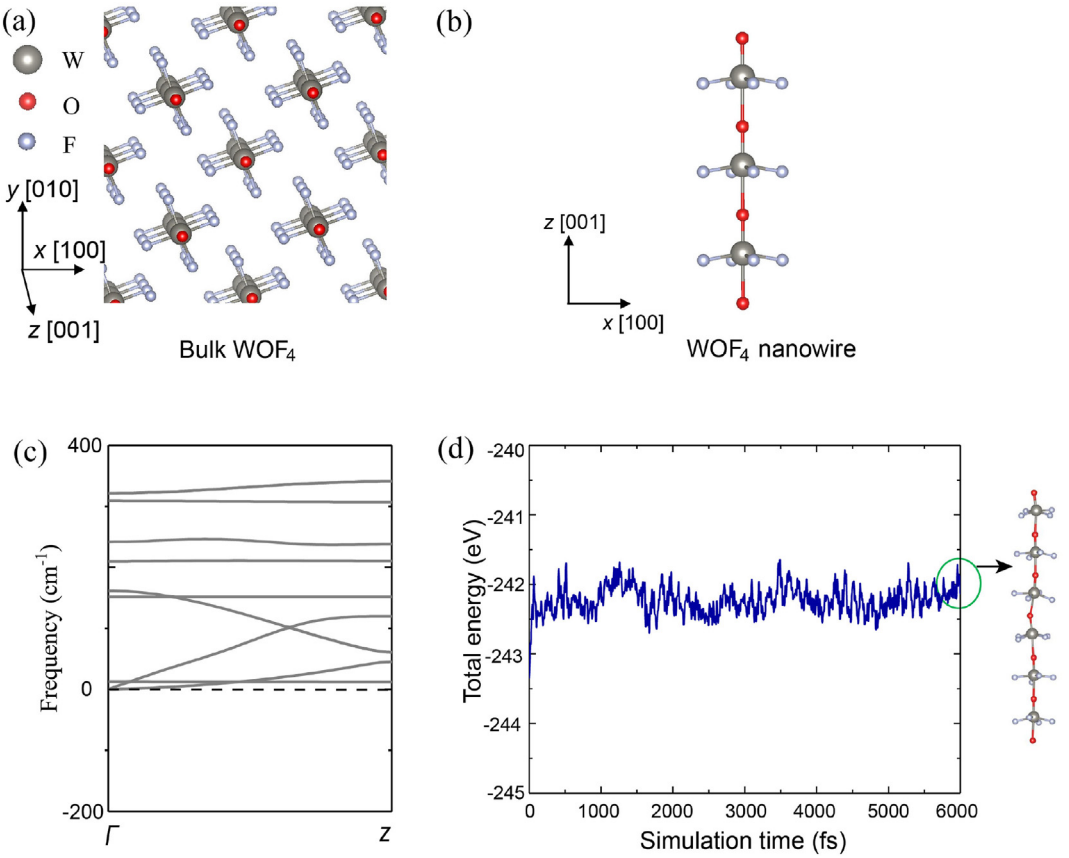

Fig. 1. Lattice structures of (a) bulk WOF_4 and (b) WOF_4 nanowire; (c) phonon dispersion curves of WOF_4 nanowire; (d) The *ab initio* MD simulations performed at 300 K.

circumvents the well-known restriction of critical thicknesses problem in traditional ferroelectrics caused by the increased depolarization effects that accompany size reductions. As illustrated in Fig. 2(a), the distorted ***F*** phase can transform into symmetry-equivalent ***F***′ ground-states with opposite distortion value *via* a spatial inversion operation. As a result, the ***F*** and ***F***′ phases have opposite polarizations. In the intermediate state between them (a space group of *P*4/*m*), the WOF_4 nanowire retains the centrosymmetry with $\boldsymbol{d} = 0$, which forbids the existence of ferroelectricity, and the lattice parameter is calculated to be 3.80 Å. The variation in the energy of the structure versus the normalized distortion displacement is also calculated, which manifests itself as obvious double well potential characteristics. The results clearly signal that the WOF_4 is an intrinsic 1D ferroelectric.

The polarization P_s of the nanowire is confirmed and calculated by the standard Berry phase approach (see Fig. 2(b)). Note that the polarization of low-dimensional material depends on the estimation of the unit cell volume. Here we employ the vdW interchain spacing of bulk WOF_4 d_0 to estimate the volume of the nanowire. The obtained spontaneous polarization is equivalent to 49.03 μC/cm^2 along the axial direction, which is slightly smaller than the corresponding value of 52.89 μC/cm^2 in bulk WOF_4. This value is larger than those of recently predicted 1D nanowires [18], and is the same order as that of bulk ferroelectric $PbTiO_3$ (~85.8 μC/cm^2) [42], indicating that the WOF_4 nanowire is a potential excellent 1D FE material. The large polarization is originated from the large displacement of the F atoms with respect to the W atoms as well as their sizable electronegative difference. To inspect the feasibility of polarization reversion, we further investigate the minimum energy pathway for the polarization transition from the ***F*** to ***F***′ phase using the CI-NEB methods. The results are illustrated in Fig. 2(c). One can see that the transition pathway goes through an intermediate paraelectric phase and the overall transition barrier (E_b) is about 0.38 eV. This value is in the same order as those in traditional ferroelectric oxides, such as 0.1–0.2 eV·f.u.$^{-1}$ for $PbTiO_3$, and some low-dimensional ferroelectric materials [43,44]. This large E_b ensures the robustness of the ferroelectricity in the nanowire at room temperature. It is also worth mentioning that the ferroelectricity is confirmed to be preserved at 300 K from our AIMD simulations. These results unveil that the WOF_4 nanowire is intrinsic room-temperature ferroelectrics.

The stability of the ferroelectricity against finite temperature effect is quantitatively measured by the Curie transition temperatures T_C, above which spontaneous polarization vanishes. We employ the Monte Carlo (MC) method to estimate the T_C. The free energy of the WOF_4 nanowire can be constructed as:

$$E = E_{FE}(d) + E_{elas}(\eta) + E_{int}(d, \eta) \quad (1)$$

Here, the first term E_{FE} describes the energy arises from the ferroelectric distortion associated with the displacement of W atom d, E_{elas} is the elastic energy, and $E_{int}(d, \eta)$ describes the coupling between ferroelectric distortion and strain η. Based on the constructed model, the Monte Carlo simulation with Metropolis algorithm is introduced to investigate the finite temperature properties of WOF_4 nanowire. At each MC step, we make a trial move on each degrees of freedom, and the change of energy ΔE can be calculated through Eq. (1). The possibility of this move can be calculated by $p = \min\left(1, e^{-\frac{\Delta E}{k_B T}}\right)$, where k_B is Boltzmann constant. The equilibrate state under 0 K is achieved with 10^5 MC sweeps, after that, the

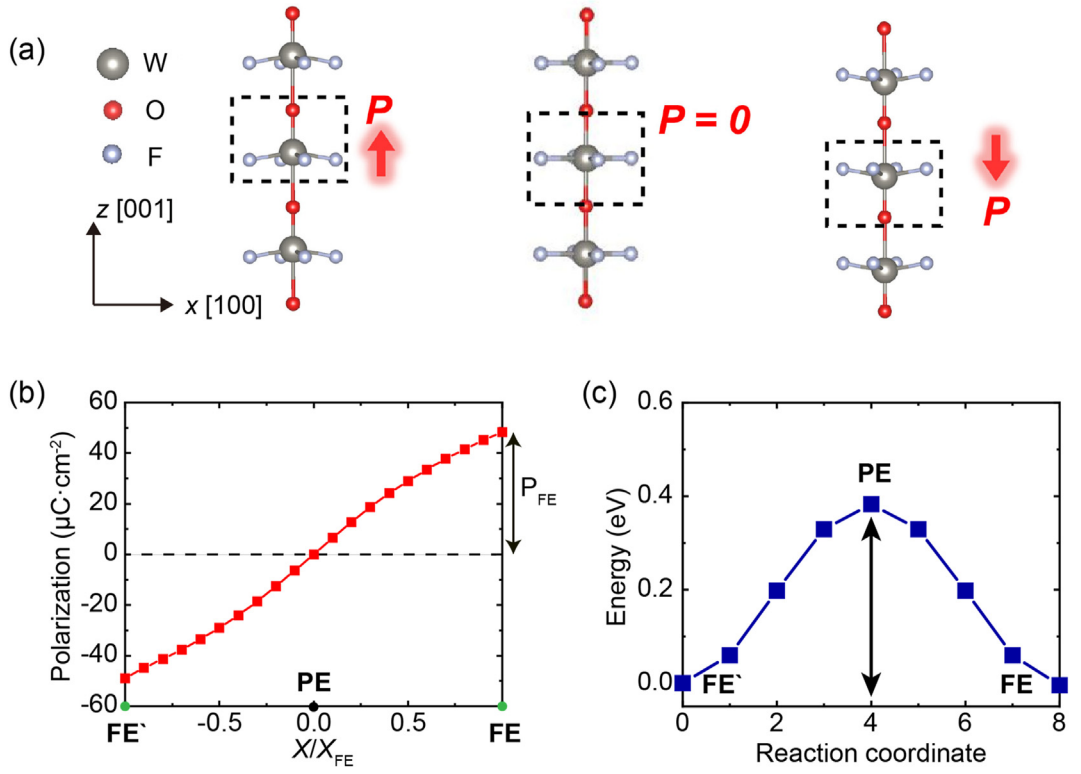

Fig. 2. (a) Atomic structures of the two energy-degenerate distorted polar phases (***F*** and ***F***') and the undistorted phase ***P***; (b) polarization of WOF_4 obtained from the Berry phase method; (c) Minimum energy pathway and energy barrier for the polarization switching.

model is heated up to 2 500 K with a temperature step of 1 K. For each temperature step, 10^5 MC sweeps are performed. Fig. 3 shows the temperature dependence of ferroelectric distortion of the nanowire obtained by the MC simulations, which indicates that the T_C value is around 1 250 K. The above results demonstrate that the WOF_4 nanowire is intrinsic room-temperature ferroelectrics.

3.3. Strain effect

The low dimensional structures are normally fabricated on a substrate or grow in carbon nanotubes [38] with inevitable misfit strain. To probe the strain modulations of the ferroelectricity of the nanowire, we apply the axial strain ε to the nanowire. The quantity is defined as $\varepsilon = (c - c_0)/c_0$ with c as the lattice constant along the axial direction for the strained structure. Fig. 4 shows the evolution of polarization and the activation barrier for the ferroelectric transition with applied strain. We can see that the polarization increases almost linearly from 49.03 μC/cm^2 to 55.68 μC/cm^2 as the axial tension increases from 0 to 4%, while decreases rapidly to about 37.01 μC/cm^2 at a 4% compressive strain. Besides, the energy barrier is also sensitive to mechanical strain, which reaches 0.82 eV at 4% of the tensile strain and decreases to 0.11 eV at 4% of the compressive strain. Therefore, the ferroelectricity of 1D WOF_4 can be effectively modulated by the application of strain engineering, which has also been found in bulk and 2D ferroelectrics [45,46].

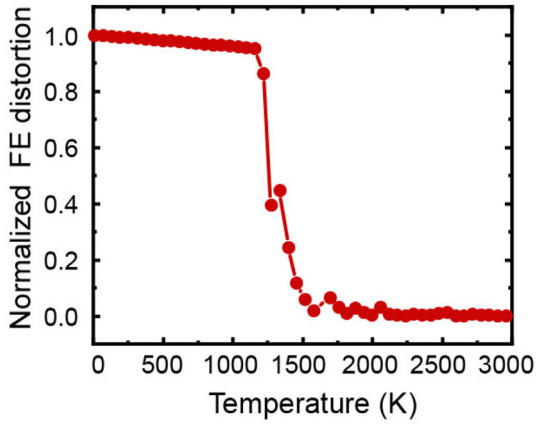

Fig. 3. Normalized averaged ferroelectric distortion of the WOF_4 nanowire as a function of temperature obtained from the MC simulations.

3.4. Doping effect

We further investigate the effect of electrostatic doping on the ferroelectric and electronic properties of the nanowire using the HSE06 hybrid functional, which is expected to describe the atomic structures and electronic structures of wide band gap oxides more accurately. Previous studies have reported that excess electrons are detrimental to ferroelectricity in bulk ferroelectrics due to the screening effect, which results in the disappearance of polar distortion at high electron density (*e.g.* 0.085 e/f.u. in $BaTiO_3$ [47]). The evolution of ferroelectric properties in the nanowire as reflected by the polar displacements versus electrostatic doping is shown in Fig. 5(a). Surprisingly, the ferroelectric structure remains stable throughout the whole doping density range. The polar displacements maintain a relatively large value and even increase with increasing doping holes or electrons, in stark contrast to conventional ferroelectric $BaTiO_3$ which shows a sharp decreasing trend upon electron doping. These results manifest that the robust polar ordering survives the free carriers doping and there is no critical doping density for the absence of ferroelectricity in the ferroelectric

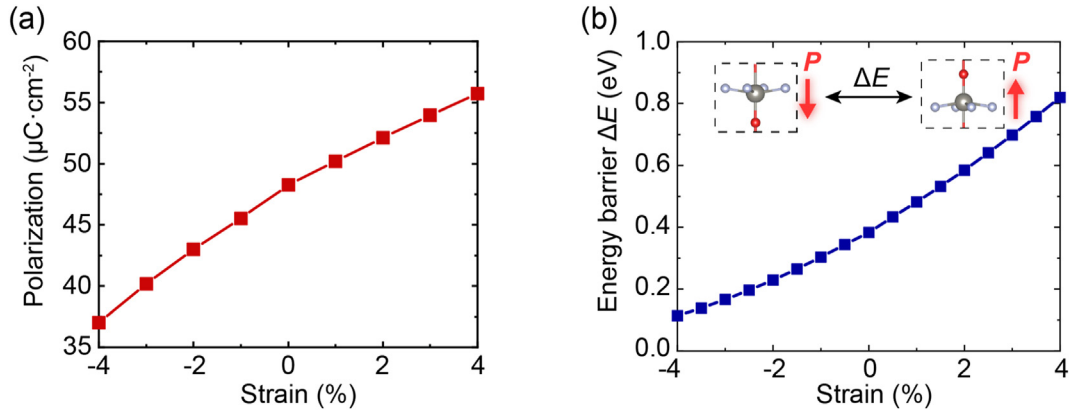

Fig. 4. Strain-dependent (a) polarization and (b) energy barrier for the WOF_4 nanowire.

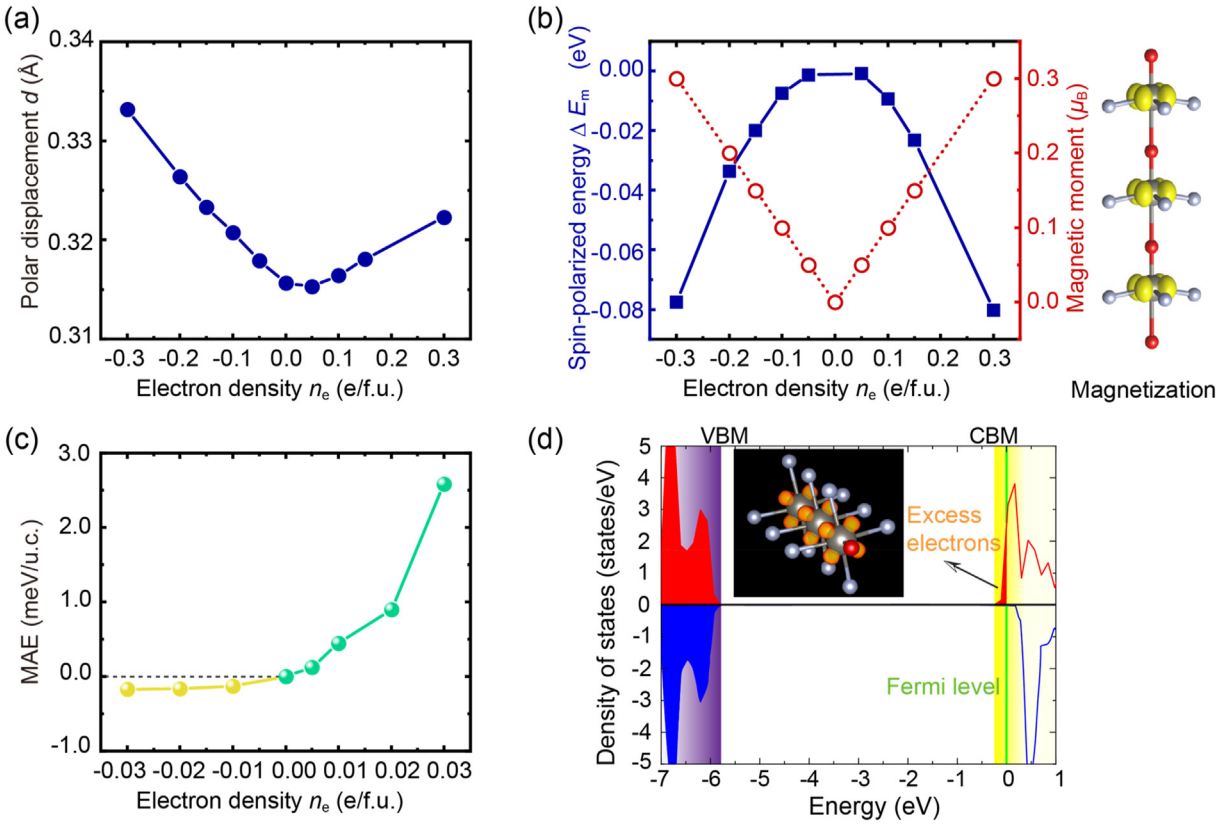

Fig. 5. Metallic multiferroic properties of free-carriers doped WOF_4 nanowire. The doping density dependence of (a) ferroelectric displacement *d*, (b)spin-polarized energyΔE_m, magnetic moments, and (c) MAE of the nanowire; (d) density of states with doping electron of 0.01 e/f.u. The green solid line is the Fermi level. The squared wave functions of the excess electrons are shown in the right panel.

WOF_4 nanowire.

More interestingly, we found that doped free carriers are also associated with magnetism in the nanowire. Fig. 5(b) illustrates the doping density dependence of the spin-polarized energy ΔE_m defined as the energy difference between the ferromagnetic and nonmagnetic states, $\Delta E_m = E_{FM}$-E_{NM}. The ferromagnetic state is unstable at $n_e = 0$ due to the absence of excess charge. The negative values indicate that magnetism is activated immediately upon doping, despite the fact that ferroelectric WOF_4 nanowire is intrinsically nonmagnetic. The magnetization density distribution for the electron doping concentration of $n_e = 0.01$ e·f.u.$^{-1}$ is visualized in the right part of Fig. 5(b). We can clearly find that the magnetization is particularly confined around the W atoms. The 1D magnetism becomes more stable and the emerging magnetic moments increase linearly with increasing doping density. Moreover, we calculate the magnetic anisotropy energy (MAE) of the magnetic nanowire as a function of doping density by considering spin-orbit coupling. Herein, the MAE is defined as the energy difference between the magnetic moment aligned along the [001] axis and in the (001) plane, *i.e.* MAE = $E_{[001]}$-$E_{(001)}$, since the energy is found to be insensitive to spin directions within (001) plane. As shown in Fig. 5(c), the MAE is positive in electron doping and increases with increasing electron density, indicating that the (001) plane is the easy magnetization plane. Specifically, we obtain the MAE of

0.45 meV/unit cell for $n_e = 0.01$ e·f.u.$^{-1}$, which is comparable with those of many intrinsic monolayer ferromagnets [48,49]. The hole doping plays an opposite effect on the MAE, with the easy magnetization axis along the [001] due to the negative MAE, although the value is much smaller. Thus, the magnetization orientation turns from in-plane to axial direction with hole doping, suggesting the possibility of controlling magnetoelectric coupling with doping concentration. We further calculate the electronic properties of the doped nanowire. The spin-polarized density of states (DOS) of the system at $n_e = 0.01$ e·f.u.$^{-1}$ (see Fig. 5(d)) displays a clear ferromagnetic metallic state, as the majority spin crosses the Fermi level containing a smaller portion of occupied electrons with respect to the minority spin. As visualized from the squared wave functions, the spin-polarized excess electrons are primarily contributed by d_{xy} orbitals of W atoms, which contribute to magnetism and electrical conduction in the system.

The above results thus present the nontrivial coexistence of polar distortion, magnetism, and conductivity in the doped WOF_4 nanowire. The stable WOF_4 atomic wire displays robust intrinsic ferroelectricity attributed to the large cooperative atomic displacements. Despite being intrinsically nonmagnetic and insulating, upon free-carriers injection, ferroelectric WOF_4 nanowire simultaneously exhibits multiferroic and conducting properties. The present design strategy based on the doping of 1D ferroelectrics circumvents the conventional restrictions between ferroelectricity and conductivity as well as between ferroelectric and magnetic properties in the extremely fine size, providing a means to the search for entirely new 1D multiferroic semiconductors. In addition to the conceptual significance, the integrated multiferroic and conductive properties in the atomic-scale nanowire provide a plethora of fascinating and innovative applications in the field of nanoscale electronics, such as magnetoelectricity [50], electrocatalysis [51], and photovoltaics [52]. The unusual coexistence of these seemingly “conflicting” properties in a single-phase material also offers a new platform to explore unique physical phenomena such as superconductivity [53,54], unusual optical properties [55,56], and enhanced thermoelectric properties [57].

4. Conclusion

In summary, we demonstrate that the WOF_4 nanowire is an intrinsic 1D ferroelectric with robust axial spontaneous polarization by using first-principles calculations. The energetic, dynamical, and thermodynamic stabilities of the nanowire have been confirmed theoretically. The nanowire exhibits robust ferroelectricity with a large spontaneous polarization value and a high Curie transition temperature, as a result of large relative atomic displacements. Furthermore, the ferroelectric distortion persists with free carriers in the nanowire. The doping electrons are in spin-polarized states, giving rise to ferromagnetic metallic states. Our findings not only broaden the family of 1D ferroelectrics but also present a new concept and approach for 1D metallic multiferroics.

Data availability

The data that support the findings of this study are available from the corresponding authors upon reasonable request.

Declaration of competing interest

The authors declare that they have no known competing financial interests or personal relationships that could have appeared to influence the work reported in this paper.

Acknowledgments

The work is supported by the National Natural Science Foundation of China (Grant Nos. 12172370, 11874059 and 12174405), Natural Science Foundation of Zhejiang Provincial (Grant Nos.LY22E020012 and LR19A040002), National Key R&D Program of China (Grant No.2022YFB3807601) , the Key Research Project of Zhejiang Laboratory (Grant No. 2021PE0AC02), Zhejiang Laboratory Open Research Project (Grant No. K2022PE0AB06) and JSPS International Research Fellow (No. P22065).

Appendix A. Supplementary data

Supplementary data to this article can be found online at https://doi.org/10.1016/j.jmat.2023.02.012.

References

[1] Lines ME, Glass AM, Burns G. Principles and applications of ferroelectrics and related materials. Phys Today 1978;31:56–8. https://doi.org/10.1063/1.2995188.
[2] Scott JF. Ferroelectric memories. first ed. Heidelberg: Springer Berlin; 2000. https://doi.org/10.1007/978-3-662-04307-3.
[3] Ali T, Lehninger D, Lederer M, Li S, Kühnel K, Mart C, et al. Tuning hyrbrid ferroelectric and antiferroelectric stacks for low power FeFET and FeRAM applications by using laminated HSO and HZO films. Adv Electron Mater 2022;8:2100837. https://doi.org/10.1002/aelm.202100837.
[4] Nahas Y, Prokhorenko S, Louis L, Gui Z, Kornev I, Bellaiche L. Discovery of stable skyrmionic state in ferroelectric nanocomposites. Nat Commun 2015;6:8542. https://doi.org/10.1038/ncomms9542.
[5] Shimada T, Xu T, Uratani Y, Wang J, Kitamura T. Unusual multiferroic phase transitions in $PbTiO_3$ nanowires. Nano Lett 2016;16:6774–9. https://doi.org/10.1021/acs.nanolett.6b02370.
[6] Wang J, Xu T, Shimada T, Wang X, Zhang TY, Kitamura T. Chiral selectivity of improper ferroelectricity in single-wall $PbTiO_3$ nanotubes. Phys Rev B 2014;89:144102. https://doi.org/10.1103/PhysRevB.89.144102.
[7] Cheema SS, Kwon D, Shanker N, dos Reis R, Hsu SL, Xiao J, et al. Enhanced ferroelectricity in ultrathin films grown directly on silicon. Nature 2020;580:478–82. https://doi.org/10.1038/s41586-020-2208-x.
[8] Liu J, Ji Y, Yuan S, Ding L, Chen W, Zheng Y. Controlling polar-toroidal multi-order states in twisted ferroelectric nanowires. NPJ Comput Mater 2018;4:78. https://doi.org/10.1038/s41524-018-0135-2.
[9] Naumov II, Bellaiche L, Fu H. Unusual phase transitions in ferroelectric nanodisks and nanorods. Nature 2004;432:737–40. https://doi.org/10.1038/nature03107.
[10] Polking MJ, Han MG, Yourdkhani A, Petkov V, Kisielowski CF, Volkov VV, et al. Ferroelectric order in individual nanometre-scale crystals. Nat Mater 2012;11:700–9. https://doi.org/10.1038/nmat3371.
[11] Chang K, Liu J, Lin H, Wang N, Zhao K, Zhang A, et al. Discovery of robust in-plane ferroelectricity in atomic-thick SnTe. Science 2016;353:274–8. https://doi.org/10.1126/science.aad8609.
[12] Manzeli S, Ovchinnikov D, Pasquier D, Yazyev OV, Kis A. 2D transition metal dichalcogenides. Nat Rev Mater 2017;2:17033. https://doi.org/10.1038/natrevmats.2017.33.
[13] Hu Z, Ding Y, Hu X, Zhou W, Yu X, Zhang S. Recent progress in 2D group IV–IV monochalcogenides: synthesis, properties and applications. Nanotechnology 2019;30:252001. https://doi.org/10.1088/1361-6528/ab07d9.
[14] Di Sante D, Stroppa A, Barone P, Whangbo MH, Picozzi S. Emergence of ferroelectricity and spin-valley properties in two-dimensional honeycomb binary compounds. Phys Rev B 2015;91:161401. https://doi.org/10.1103/PhysRevB.91.161401.
[15] Liu M, Artyukhov VI, Yakobson BI. Mechanochemistry of one-dimensional boron: structural and electronic transitions. J Am Chem Soc 2017;139:2111–7. https://doi.org/10.1021/jacs.6b12750.
[16] Park C, Kim SW, Yoon M. First-principles prediction of new electrides with nontrivial band topology based on one-dimensional building blocks. Phys Rev Lett 2018;120:026401. https://doi.org/10.1103/PhysRevLett.120.026401.
[17] Tang ZK, Zhang L, Wang N, Zhang XX, Wen GH, Li GD, et al. Superconductivity in 4 angstrom single-walled carbon nanotubes. Science 2001;292:2462–5. https://doi.org/10.1126/science.106047.
[18] Yang C, Chen M, Li S, Zhang X, Hua C, Bai H, et al. Coexistence of ferroelectricity and ferromagnetism in one-dimensional SbN and BiN nanowires. ACS Appl Mater Interfaces 2021;13:13517–23. https://doi.org/10.1021/acsami.0c20570.
[19] Zhang L, Tang C, Sanvito S, Du A. Purely one-dimensional ferroelectricity and antiferroelectricity from van der Waals niobium oxide trihalides. NPJ Comput Mater 2021;7:135. https://doi.org/10.1038/s41524-021-00602-9.
[20] Zhang JJ, Guan J, Dong S, Yakobson BI. Room-temperature ferroelectricity in group-IV metal chalcogenide nanowires. J Am Chem Soc 2019;141:15040–5.

https://doi.org/10.1021/jacs.9b03201.
[21] Kresse G, Hafner J. Ab initio molecular dynamics for liquid metals. Phys Rev B 1993;47:558–61. https://doi.org/10.1103/PhysRevB.47.558.
[22] Kresse G, Furthmüller J. Efficient iterative schemes for ab initio total-energy calculations using a plane-wave basis set. Phys Rev B 1996;54:11169–86. https://doi.org/10.1103/PhysRevB.54.11169.
[23] Grimme S. Semiempirical GGA-type density functional constructed with a long-range dispersion correction. J Comput Chem 2006;27:1787–99. https://doi.org/10.1002/jcc.20495.
[24] Ernzerhof M, Scuseria GE. Assessment of the perdew–burke–ernzerhof exchange-correlation functional. J Chem Phys 1999;110:5029–36. https://doi.org/10.1063/1.478401.
[25] Heyd J, Scuseria GE, Ernzerhof M. Hybrid functionals based on a screened Coulomb potential. J Chem Phys 2003;118:8207–15. https://doi.org/10.1063/1.1564060.
[26] Heyd J, Scuseria GE, Ernzerhof M. Erratum: “hybrid functionals based on a screened coulomb potential” [J chem phys 2003;118:8207]. J Chem Phys 2006;124:219906. https://doi.org/10.1063/1.2204597.
[27] Oba F, Togo A, Tanaka I, Paier J, Kresse G. Defect energetics in ZnO: a hybrid Hartree-Fock density functional study. Phys Rev B 2008;77:245202. https://doi.org/10.1103/PhysRevB.77.245202.
[28] Shimada T, Ueda T, Wang J, Kitamura T. Hybrid Hartree-Fock density functional study of charged point defects in ferroelectric $PbTiO_3$. Phys Rev B 2013;87:174111. https://doi.org/10.1103/PhysRevB.87.174111.
[29] Xu T, Shimada T, Araki Y, Wang J, Kitamura T. Defect-strain engineering for multiferroic and magnetoelectric properties in epitaxial (110) ferroelectric lead titanate. Phys Rev B 2015;92:104106. https://doi.org/10.1103/PhysRevB.92.104106.
[30] Janotti A, Varley JB, Rinke P, Umezawa N, Kresse G, Van de Walle CG. Hybrid functional studies of the oxygen vacancy in TiO_2. Phys Rev B 2010;81:085212. https://doi.org/10.1103/PhysRevB.81.085212.
[31] Shimada T, Xu T, Araki Y, Wang J, Kitamura T. Unusual metallic multiferroic transitions in electron-doped $PbTiO_3$. Adv Electron Mater 2017;3:1700134. https://doi.org/10.1002/aelm.201700134.
[32] Henkelman G, Jónsson H. Improved tangent estimate in the nudged elastic band method for finding minimum energy paths and saddle points. J Chem Phys 2000;113:9978–85. https://doi.org/10.1063/1.1323224.
[33] Togo A, Oba F, Tanaka I. First-principles calculations of the ferroelastic transition between rutile-type and $CaCl_2$-type SiO_2 at high pressures. Phys Rev B 2008;78:134106. https://doi.org/10.1103/PhysRevB.78.134106.
[34] Jain A, Ong SP, Hautier G, Chen W, Richards WD, Dacek S, et al. Commentary: the Materials Project: a materials genome approach to accelerating materials innovation. Apl Mater 2013;1:011002. https://doi.org/10.1063/1.4812323.
[35] Cheon G, Duerloo KAN, Sendek AD, Porter C, Chen Y, Reed EJ. Data mining for new two- and one-dimensional weakly bonded solids and lattice-commensurate heterostructures. Nano Lett 2017;17:1915–23. https://doi.org/10.1021/acs.nanolett.6b05229.
[36] Lu F, Cui J, Liu P, Lin M, Cheng Y, Liu H, et al. High-throughput identification of one-dimensional atomic wires and first principles calculations of their electronic states. Chin Phys B 2021;30:057304. https://doi.org/10.1088/1674-1056/abdb1a.
[37] Lin LF, Zhang Y, Moreo A, Dagotto E, Dong S. Quasi-one-dimensional ferroelectricity and piezoelectricity in WOX_4 halogens. Phys Rev Mater 2019;3:111401. https://doi.org/10.1103/PhysRevMaterials.3.111401.
[38] Vasylenko A, Marks S, Wynn JM, Medeiros PVC, Ramasse QM, Morris AJ, et al. Electronic structure control of sub-nanometer 1D SnTe via nanostructuring within single-walled carbon nanotubes. ACS Nano 2018;12:6023–31. https://doi.org/10.1021/acsnano.8b02261.
[39] Zhuang HL, Hennig RG. Computational search for single-layer transition-metal dichalcogenide photocatalysts. J Phys Chem C 2013;117:20440–5. https://doi.org/10.1021/jp405808a.
[40] Xu T, Shimada T, Araki Y, Mori M, Fujimoto G, Wang J, et al. Electron engineering of metallic multiferroic polarons in epitaxial $BaTiO_3$. NPJ Comput Mater 2019;5:23. https://doi.org/10.1038/s41524-019-0163-6.
[41] Shimada T, Xu T, Araki Y, Wang J, Kitamura T. Multiferroic dislocations in ferroelectric $PbTiO_3$. Nano Lett 2017;17:2674–80. https://doi.org/10.1021/acs.nanolett.7b00505.
[42] Shimada T, Umeno Y, Kitamura T. Ab initio study of stress-induced domain switching in $PbTiO_3$. Phys Rev B 2008;7:094105. https://doi.org/10.1103/PhysRevB.77.094105.
[43] Samad A, Kim HJ, Shin YH. Stability, spontaneous and induced polarization in monolayer MoC, WC, WS, and WSe. J Phys Condens Matter 2018;31:045301. https://doi.org/10.1088/1361-648X/aaf14d.
[44] Liu Z, Sun Y, Singh DJ, Zhang L. Switchable out-of-plane polarization in 2D $LiAlTe_2$. Adv electron mater 2019;5:1900089. https://doi.org/10.1002/aelm.201900089.
[45] Janolin PE. Strain on ferroelectric thin films. J Mater Sci 2009;44:5025–48. https://doi.org/10.1007/s10853-009-3553-1.
[46] Xu T, Wang X, Mai J, Zhang J, Wang J, Zhang TY. Strain engineering for 2D ferroelectricity in lead chalcogenides. Adv Electron Mater 2020;6:1900932. https://doi.org/10.1002/aelm.201900932.
[47] Iwazaki Y, Suzuki T, Mizuno Y, Tsuneyuki S. Doping-induced phase transitions in ferroelectric $BaTiO_3$ from first-principles calculations. Phys Rev B 2012;86:214103. https://doi.org/10.1103/PhysRevB.86.214103.
[48] Liang J, Wang W, Du H, Hallal A, Garcia K, Chshiev M. Very large Dzyaloshinskii-Moriya interaction in two-dimensional Janus manganese dichalcogenides and its application to realize skyrmion states. Phys Rev B 2020;101:184401. https://doi.org/10.1103/PhysRevB.101.184401.
[49] Miao N, Xu B, Zhu L, Zhou J, Sun Z. 2D intrinsic ferromagnets from van der Waals antiferromagnets. J Am Chem Soc 2018;140:2417–20. https://doi.org/10.1021/jacs.7b12976.
[50] Eerenstein W, Mathur ND, Scott JF. Multiferroic and magnetoelectric materials. Nature 2006;442:759–65. https://doi.org/10.1038/nature05023.
[51] Ke C, Huang J, Liu S. Two-dimensional ferroelectric metal for electrocatalysis. Mater Horiz 2021;8:3387–93. https://doi.org/10.1039/D1MH01556G.
[52] Grinberg I, West DV, Torres M, Gou G, Stein DM, Wu L, et al. Perovskite oxides for visible-light-absorbing ferroelectric and photovoltaic materials. Nature 2013;503:509–12. https://doi.org/10.1038/nature12622.
[53] Bauer E, Rogl G, Chen XQ, Khan RT, Michor H, Hilscher G, et al. Unconventional superconducting phase in the weakly correlated noncentrosymmetric Mo_3Al_2C compound. Phys Rev B 2010;82:064511. https://doi.org/10.1103/PhysRevB.82.064511.
[54] Bauer E, Sigrist M. Non-centrosymmetric superconductors. first ed. Heidelberg: Springer Berlin; 2012. https://doi.org/10.1007/978-3-642-24624-1.
[55] Mineev VP, Yoshioka Y. Optical activity of noncentrosymmetric metals. Phys Rev B 2010;81:094525. https://doi.org/10.1103/PhysRevB.81.094525.
[56] Edelstein VM. Features of light reflection off metals with destroyed mirror symmetry. Phys Rev B 2011;83:113109. https://doi.org/10.1103/PhysRevB.83.113109.
[57] Puggioni D, Rondinelli JM. Designing a robustly metallic noncenstrosymmetric ruthenate oxide with large thermopower anisotropy. Nat Commun 2014;5:3432. https://doi.org/10.1038/ncomms4432.

Tao Xu was born in 1988, in Shaoxing, Zhejiang, China. He received his Ph.D. degree from the Department of Mechanical Engineering and Science, Kyoto University, Kyoto, Japan, in 2017. He is currently Associated Professor in Ningbo Institute of Materials Technology and Engineering, Chinese Academy of Sciences, and a JSPS Fellow in Kyoto University. His research interests are multi-scale calculations on ferroelectrics and multiferroics. He has worked on more than 5 research programs. He has published more than 30 papers.